JOURNAL OF GEOPHYSICAL RESEARCH, VOL. 113, C03014, doi:10.1029/2007JC004134, 2008

Role of gyration in the oceanic general circulation: Atlantic Ocean

Hua Jiang,[1] Rui Xin Huang,[2] and Hui Wang[1]

Received 28 January 2007; revised 27 October 2007; accepted 4 December 2007; published 14 March 2008.

[1] Wind-driven gyres transport volume and heat in the meridional direction, which is an important component of the climate system. The contribution of wind-driven gyres to both poleward volume and heat fluxes can be clearly identified from numerical models by a simple diagnostic tool; thus the central location, strength, and dynamical roles of wind-driven circulation in the climatological mean state and decadal variability of the oceanic circulation can be examined in detail. This diagnostic tool was applied to the Simple Ocean Data Assimilation data generated from a numerical model, with data assimilation. Our analysis indicates the important contribution due to wind-driven gyres and the strong decadal variability in the volume flux, heat flux, and central location of the wind-driven gyres in the Atlantic Ocean.

Citation: Jiang, H., R. X. Huang, and H. Wang (2008), Role of gyration in the oceanic general circulation: Atlantic Ocean, *J. Geophys. Res.*, *113*, C03014, doi:10.1029/2007JC004134.

1. Introduction

[2] Oceans play critical roles in transporting mass and heat fluxes meridionally through water mass formation and transformation processes, which are important factors in climate changes [*Levitus*, 1989a, 1989b; *Greatbatch et al.*, 1991; *Kushnir*, 1994; *Molinari et al.*, 1997; *Talley*, 2003]. The three-dimensional oceanic circulation can be classified into two major components: the wind-driven circulation and the thermohaline circulation. Traditionally, the diagnosis of these circulations is based on the meridional stream function map, obtained by integrating the meridional velocity in the zonal direction.

[3] This interpretation of oceanic transports is somewhat limiting. First, the deep flow in the ocean interior is different from what is implied by the zonally integrated meridional stream function map. Second, the location and the value of the maximal volume flux from the meridional stream function map provide an incomplete description of the circulation only. Third, the meridional stream function map does not provide much information about the three-dimensional structure of the circulation. In fact, the horizontal wind-driven circulation is excluded from such a map. Although using the meridional overturning stream function defined in terms of potential temperature or potential density coordinates may provide better information about the oceanic circulation, such stream function maps have similar shortcomings to those discussed above.

[4] There have been a few studies in which the role of barotropic gyration were separated as individual items to interpret the oceanic heat transport [*Bryden and Hall*, 1980; *Bryan*, 1982; *Sarmiento*, 1986; *Semtner and Chervin*, 1988; *Brady*, 1994a, 1994b; *Fanning and Weaver*, 1997]. For example, *Bryan* [1982] separated the heat transport into overturning, gyre, seasonal-overturning, and eddy-mixing components in a coarse-resolution model. The net equatorward heat transport associated with the horizontal gyre-like circulation around the Pacific equatorial upwelling zone was analyzed by *Brady* [1994a, 1994b] and *Fanning and Weaver* [1997] decomposed the oceanic heat transport into its baroclinic overturning, barotropic gyre, and baroclinic components in their idealized coupled climate model.

[5] To understand the oceanic role in the climate system, a new and simpler diagnostic tool for the meridional volume and heat transports by the horizontal wind-driven gyres will be introduced in this paper. This tool can be used to diagnose the central location (in depth and latitude), meridional volume, and heat transports of each individual gyre in the oceans and the corresponding variability. Five important gyres in the Atlantic will be discussed, using the new diagnostic tool based on the Simple Ocean Data Assimilation (SODA) package version 7 of *Carton et al.* [2000a, 2000b]: two Subtropical gyres, the Subpolar Gyre, the Angola Gyre (Angola Dome) in the South Atlantic, and the Guinea Gyre (Guinea Dome) in the North Atlantic. The North (South) Subtropical Gyre and the Subpolar Gyre are strong and have been discussed in many studies. In comparison, volume transport of the Angola Gyre and the Guinea Gyre is small and not well documented. The North Subtropical Gyre has strong decadal variability. Observed subsurface variations of temperature and salinity show a major shift in the North Atlantic Ocean circulation between the late 1950s and the early 1970s [*Levitus*, 1989a, 1989b]. Previous diagnostic calculations [*Greatbatch et al.*, 1991; *Ezer*, 1999] suggested that transport of the Gulf Stream in the pentad 1970–1974 was 30 Sv weaker than in the pentad

[1]Institute of Climate System, Chinese Academy of Meteorological Sciences, Beijing, China.
[2]Department of Physical Oceanography, Woods Hole Oceanographic Institute, Woods Hole, Massachusetts, USA.

0148-0227/08/2007JC004134$09.00

1955–1959 and about 20 Sv of this decline was due to a dramatic weakening of the circulation of the North Subtropical Gyre. Such changes in the circulation were mostly attributed to variability in the bottom pressure torque associated with the flow-topography interaction on the western side of the Mid-Atlantic Ridge.

[6] Using oceanographic station arrays, *Moroshkin et al.* [1970] put the central location of the Angola Gyre (Dome) at (10°S, 9°E). Using the oceanographic data obtained during 1983–1984, *Gordon and Bosley* [1991] put the center of this cyclonic gyre at (13°S, 5°E) and mostly confined to the upper 300 m, with the velocity maximum at 50 m depth. In fact, the center of the Angola Gyre can extend to 4°S in terms of the total volume transport. A model simulation [*Yamagata and Iizuka*, 1995] indicated that the Angola Gyre has seasonal variations, mainly induced by the negative surface heat flux from March to August.

[7] The climatology and seasonal variations of the Guinea Gyre (commonly called the Guinea Dome because of the shallow dome-like thermocline due to Ekman upwelling) were discussed by *Busalacchi and Picaut* [1983], *Siedler et al.* [1992], *Yamagata and Iizuka* [1995], and *Mazeika* [1967]. This gyre is located near (12°N, 22°W), with anticlockwise flow due to the eastward North Equatorial Countercurrent (NECC) and the westward North Equatorial Current (NEC). Strong seasonal variations in the southern part of the dome in the upper 150 m are related to seasonal changes in the NECC. *Siedler et al.* [1992] suggested that the Guinea Dome is driven primarily by the large-scale wind stress not by the local wind stress because the small-scale features of the Ekman pumping rate are not well correlated with the geostrophic current in the dome. However, heat content analysis of the dome demonstrates that the Guinea Dome is driven adiabatically during the boreal summer and fall by the divergence of the heat transport generated by the local positive wind stress curl [*Yamagata and Iizuka*, 1995]. Moreover, the gyre's variability on longer timescales, important for a better understanding of the equatorial thermal structure, has not been considered in previous studies.

[8] This paper is organized as follows. The data and the definition of volume and heat fluxes due to horizontal gyres are introduced in section 2. The algorithm is applied to the Atlantic Ocean and the climatological mean meridional volume and heat transports of individual gyres are discussed in section 3. The decadal variability of meridional volume transport of three major gyres in the North Atlantic are described and compared to the meridional transport calculated from the Sverdrup relation with a time delay factor in section 4. Finally, we conclude in section 5.

2. Data and Definition of the Circulation

2.1. Data

[9] Retrospective analysis of the global ocean based on the SODA package of *Carton et al.* [2000a, 2000b] with some improvements was used in this study. This is a monthly mean data with relatively low horizontal resolution of 1.5° × 2.5° at midlatitudes and 20 levels in the vertical direction, spanning the period of January 1950 to December 1999. The analysis relies on subsurface temperature and salinity from the National Oceanographic Data Center's World Ocean Atlas 1994, additional conductivity-temperature-depth and expendable bathythermograph data from the Global Temperature-Salinity Profile Program and other sources, thermistor temperature from the Tropical Atmosphere-Ocean array, in situ and satellite sea surface temperatures, and, finally, satellite altimeter sea level from Geosat, ERS-1, ERS-2, and TOPEX/POSEIDON.

2.2. Gyration in a Three-Dimensional Circulation

[10] A new tool is used in this study to diagnose the contribution of wind-driven gyre to the meridional transport of volume and heat. For simplicity the Cartesian coordinates are used for the formulation; however, the spherical coordinates are actually used in data analysis. First, for a given grid point (y_j, z_k) in the y-z plane a zonal-accumulated meridional volume flux (ZAMF) is defined

$$\psi_k(x, y_j) = \Delta z_k \int_{x_k^e}^{x} v(x, y_j, z_k)\, dx, \tag{1}$$

where Δz_k is the thickness of the given level k, $x_k^e = x_k^e(y_j, z_k)$ is the eastern boundary of the basin for this grid point. The meridional throughflow volume flux (defined as the net meridional volume flux at a given level k) for this grid point is

$$m_k^t = \psi_k(x_k^w, y_j), \tag{2}$$

where $x_k^w = x_k^w(y_j, z_k)$ is the western boundary of the basin for this grid point.

[11] Second, we search the zeros $x_{k,i}$, where $\psi_{k,i}^0(x_{k,i}) = 0$, $i = 1,2,\ldots N$. Note that $x_{k,N} \equiv x_k^e$ by definition. In general, the zero crossing of ψ is not exactly a grid point, so it is calculated by a linear interpolation. In addition, we define $x_{k,0} = x_k^w(y_j, z_k)$.

[12] Third, we search for the maximum (or minimum) within each interval $x = [x_{k,i}, x_{k,i+1}]$, $i = 0,1,2,\ldots,N-1$

$$\psi_{k,i}^m = \max_{x \in (x_{k,i}, x_{k,i+1})} \psi_k(x, y_j) \geq 0 \tag{3}$$

$$\psi_{k,i}^n = \min_{x \in (x_{k,i}, x_{k,i+1})} \psi_k(x, y_j) \leq 0. \tag{4}$$

Note that within the interval of each pair of zero there is only one extreme, either a maximum or a minimum. If it is a maximum (minimum), the corresponding value of minimum (maximum) is set to zero. By definition the location where ψ reaches the nontrivial $\psi_{k,i}^m$ and $\psi_{k,i}^n$ must be alternated. In addition, for each grid (y_j, z_k) in the y-z plane, if the throughflow is nonzero, a correction to the first value of maximum (or minimum) is needed

$$\psi_{k,1}^m = \psi_{k,1}^m - m_k^t, \quad \text{if } m_k^t > 0 \tag{5}$$

$$\psi_{k,1}^n = \psi_{k,1}^n - m_k^t, \quad \text{if } m_k^t < 0. \tag{6}$$

[13] The total meridional volume transports due to the clockwise and anticlockwise circulation for grid (y_j, z_k) are

defined as the sum of individual local minimum and maximum of ψ

$$G_k^p(y_j) = \sum_i \psi_{k,i}^m,\ G_k^n(y_j) = \sum_i \psi_{k,i}^n. \tag{7}$$

This technique can be used to diagnose all gyres (or large eddies) at given levels separately. At each latitude y the total contribution due to gyration is defined as

$$M_g(y) = \sum_{k=1}^{K} \left[|G_k^n| + G_k^p\right], \tag{8}$$

where K is the maximal number of level at this latitude. The meridional throughflow rate M_t, i.e., the net contribution due to throughflow, is

$$M_t(y) = \sum_{k=1,\, m_k^t>0}^{K} m_k^t. \tag{9}$$

The total meridional circulation rate is defined as

$$M_c(y) = M_g(y) + M_t(y). \tag{10}$$

Since the vertical grids are uneven, in order to show the volume flux over certain depth range, we rescale the volume flux in each layer as

$$G_k^{p\prime} = G_k^p \frac{h_0}{\Delta z_k},\ G_k^{n\prime} = G_k^n \frac{h_0}{\Delta z_k}, \tag{11}$$

Where h_0 = 100 m is the typical scale for most important features associated with gyre-scale circulation.

[14] In comparison the commonly used meridional overturning circulation (MOC) stream function is defined as the vertical integration

$$\psi_{\mathrm{MOC}}(y,k) = \sum_{kk=1}^{k} m_{kk}^t, \tag{12}$$

Where $m_k^t = \psi_k(x_k^w, y_j)$ is the meridional throughflow volume flux defined above. Thus the MOC stream function includes both positive and negative contributions from m_{kk}^t. On the other hand, the meridional throughflow rate M_t accounts for the positive contribution term only.

[15] The commonly used MOC rate is defined as

$$\Psi(y) = \max_{-H<z<0}(\psi_{\mathrm{MOC}}). \tag{13}$$

In addition, people simply quote the maximum of this flow rate around 20–50°N, and call it the MOC rate, i.e.,

$$\Psi_{\max} = \max(\Psi(y)). \tag{14}$$

[16] From these definitions it is readily seen that our definitions are different from the commonly used terms. First, the meridional throughflow rate M_t is the vertically accumulation of all positive contribution from the meridional throughflow volume flux m_k^t at each vertical level. On the other hand, the commonly used meridional stream function $\psi_{\mathrm{MOC}}(y, k)$ is the vertical integration of the meridional throughflow volume flux m_k^t; thus it includes both positive and negative contributions from different level. For the cases when multiple meridional overturning cells exist, M_t is larger than $\psi_{\mathrm{MOC}}(y, k)$. Second, the total meridional circulation rate M_c includes contribution due to horizontal gyration, so it is much larger than both the meridional throughflow rate and the commonly used MOC rate.

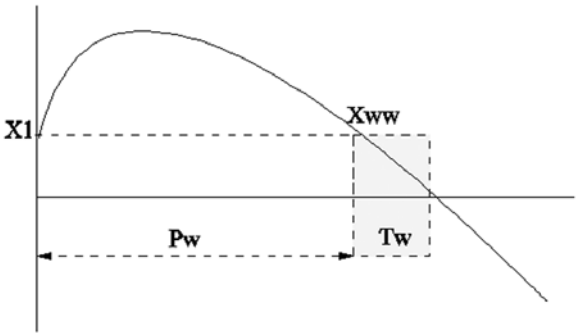

Figure 1. Sketch of the segment next to the western boundary for meridional heat transport calculation.

2.3. Heat Flux Calculation

[17] The poleward heat flux is separated into two components: throughflow and gyration. The calculation consists of three steps. First, calculate the poleward heat flux due to gyration within each pair of zero of stream function ψ: $\psi_{k,i}^0(x_{k,i}) = 0$, $i = 1,2,\ldots N$. Second, the total meridional heat flux due to the clockwise (anticlockwise) circulation for grid (y_j, z_k) is defined as the sum of individual local minimum (maximum) of ψ

$$H_k^p(y_j) = \rho_0 c_p \sum_{i=1}^{N} \int_{P_i} v\theta dx \Delta z_k \tag{15}$$

$$H_k^n(y_j) = \rho_0 c_p \sum_{j=1}^{M} \int_{N_j} v\theta dx \Delta z_k, \tag{16}$$

where $P_i(N_j)$ is the subdomain between two consequent roots of the stream function ψ, where the value ψ is positive (negative). Third, the segment next to the western boundary $x = [x_k^w, x_{k,1}]$ needs special handling, and we will discuss the case when $\psi_k^w = \psi_k(x_k^w, y_j) > 0$. There are two possible situations: First, $\psi_k^w < \psi_{k,1}^m$, where $\psi_{k,1}^m$ is the ZAMF maximum within this subdomain, and the subdomain consists of two subsegments (P_w and T_w), which are connected at x_{ww} the first point east of x_1 that satisfies $\psi = \psi_w$ (Figure 1). The heat fluxes due to throughflow and anticlockwise gyration are

$$H_k^{\mathrm{through}} = \rho_0 c_p \int_{T_W} v\theta dx \Delta z_k \tag{17}$$

$$\Delta H_k^p = \rho_0 c_p \int_{P_w} v\theta dx \Delta z_k. \tag{18}$$

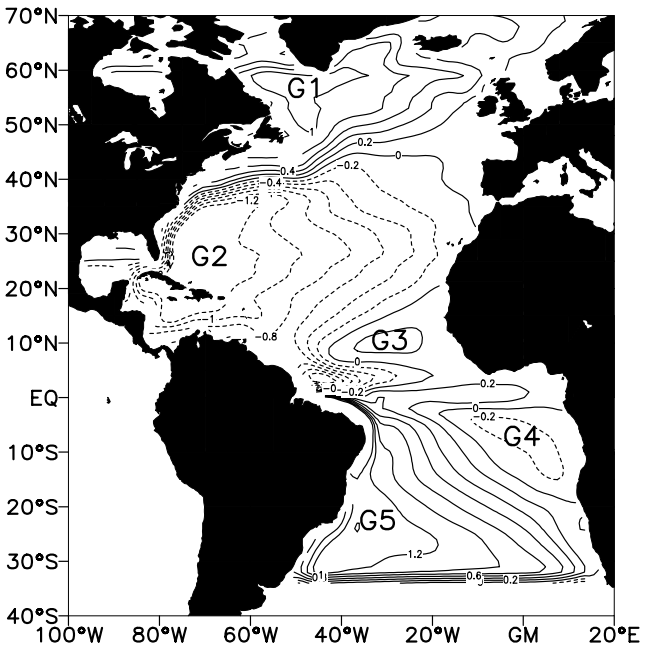

Figure 2. Climatological mean zonally integrated meridional volume transport (defined in equation (1)), at a depth of 82.5 m, the thickness of the layer is 15 m, and in units of Sv. G1 is the Subpolar Gyre, G2 is the North Subtropical Gyre, G3 is the Guinea Gyre, G4 is the Angola Gyre, and G5 is the South Subtropical Gyre.

Second, $\psi_k^w = \psi_{k,1}^m$. There is no anticlockwise flow in this segment, and heat flux contribution to the throughflow can be calculated by equation (17).

3. Gyres and Their Contribution to Meridional Fluxes in the Atlantic

3.1. Horizontal Gyres

[18] As an example, the ZAMF at depth 82.5 m in the Atlantic includes two Subtropical gyres (G2, G5), the Subpolar Gyre (G1), the anticlockwise Guinea Gyre (G3) at the latitude of Intertropical Convergence Zone due to positive Ekman pumping, and the clockwise Angola Gyre (G4) near the western coast of Africa (Figure 2). Our algorithm also provides the contribution to the meridional volume transport of each gyre (Figure 3). For example, the North Atlantic Subtropical Gyre (G2) is located within the latitudinal band of 15–45°N and in the upper 1500 m (Figure 3a). Climatological mean properties of the five most important gyres in the Atlantic Ocean are summarized in Table 1; however, discussion about the equatorial circulation is omitted.

[19] Furthermore, the maximal strength of meridional volume and heat fluxes for each gyre is identified through searching within certain latitudinal band (Table 1). The meridional position of the center of a gyre is defined as the latitude of the maximal meridional volume transport of the gyre. The vertical position of the center of an anticlockwise gyre can be defined as

$$C_z^p = \frac{\sum_{k=k_1}^{k_2}\sum_{j=j_1}^{j_2} G_k^p(y_j) z_k}{\sum_{k=k_1}^{k_2}\sum_{j=j_1}^{j_2} G_k^p(y_j)}, \qquad (19)$$

where (j_1, j_2) and (k_1, k_2) is the domain for the gyre in question, and these can be chosen suitably for each gyre. The vertical center of the clockwise gyres can be defined similarly.

3.2. Meridional Volume Fluxes

[20] The zonally integrated meridional volume transport is dominated by the North Atlantic Deep Water with southward transport of 18 Sv at most latitudes and Antarctic Bottom Water cells and the maximum overturning rate is estimated as 26 Sv at 59°N [*McCartney and Talley*, 1984; *Broecker*, 1991; *Schmitz and McCartney*, 1993; *Dickson and Brown*, 1994; *Schmitz*, 1995; *Talley et al.*, 2003]. The corresponding meridional throughflow rate diagnosed from the model is approximately 20 Sv and the commonly used term MOC rate (defined in equation (14)) is slightly larger

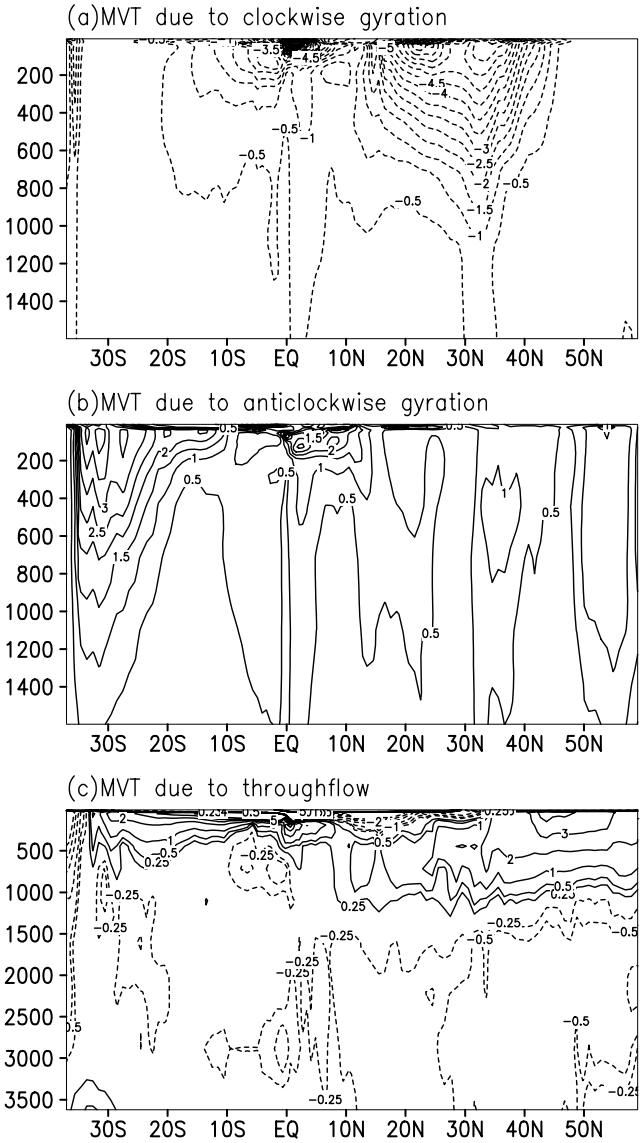

Figure 3. Meridional volume transport (MVT) as a function of latitude and depth due to (a) clockwise gyres, (b) anticlockwise gyres, and (c) throughflow for the Atlantic Ocean, in units of Sv/100 m, diagnosed from SODA data.

Table 1. Climatological Mean Location, Volume, and Heat Fluxes of Five Major Gyres in the Atlantic Ocean[a]

	Gyre G1 (Figure 3b)	Gyre G2 (Figure 3a)	Gyre G3 (Figure 3b)	Gyre G4 (Figure 3a)	Gyre G5 (Figure 3b)
Latitude	50–60°N	15–45°N	5–13°N	4–13°S	20–35°S
Depth, m	7.5–2000	7.5–2000	7.5–200	7.5–200	7.5–2000
Volume flux, Sv	25	50	5	7.5	38
Northward heat flux, PW	0.12	0.2	−0.06	0.06	−0.13

[a]G1 is the Subpolar Gyre, G2 is the North Atlantic Subtropical Gyre, G3 is the Guinea Gyre, G4 is the Angola Gyre, and G5 is the South Atlantic Subtropical Gyre.

than 10 Sv (Figure 4b). This difference between observations and the model output is due to the low horizontal resolution of the numerical model used to generate the SODA data.

[21] On the other hand, the total meridional circulation rate (equation (10)) reaches the maximum of 95 Sv at 33°N and a second maximum of 83 Sv near the equator (thick solid line in Figure 4a). Thus the total meridional circulation rate is much larger than the maximum meridional volume transport identified from the zonally integrated meridional stream function, as commonly used in diagnosing numerical model output. The essential difference is due to contributions of multiple meridional cells in the vertical plane and gyres (plus large eddies) in the horizontal plane, which may cancel each other in the calculation of the traditional overturning rate. Note that different overturning rates, defined in $y - \theta$ or $y - \sigma$ (θ is potential temperature and σ is potential density) planes, have been proposed for diagnostic study. Although such overturning rates are larger than that defined in the traditional y-z plane, they are smaller than the throughflow rate defined in this study and they cannot convey the complete information of the three-dimensional circulation.

[22] The most important feature of our algorithm is the ability to clearly identify dynamical roles of the wind-driven gyres, including their contribution to both the meridional volume and heat fluxes. There is a large contribution to the total meridional volume flux due to wind-driven gyres (thick dotted line in Figure 4a). The total amount of meridional volume flux associated with gyration has a maximum of 75 Sv around 33°N. The maximal volume fluxes of clockwise and anticlockwise circulation are associated with the North Subtropical Gyre (50 Sv) and the South Subtropical Gyre (38 Sv).

[23] In the North Atlantic, the maximal volume flux associated with the Gulf Stream recirculation system is on the order of 150 Sv [*Hogg and Johns*, 1995]. Although the SODA data was generated from a noneddy resolving model, because of the bottom pressure torque (or the so-called Joint Effect of Baroclinicity and Relief (JEBAR) term) the corresponding maximal volume transport by the Subtropical Gyre can be much larger than that because of wind stress forcing alone. For example, *Greatbatch et al.* [1991] used a $1^\circ \times 1^\circ$ model and showed that the total transport in the anticyclonic gyre in the North Atlantic Ocean reaches the maximum of approximately 60 Sv south of the Grand Banks of Newfoundland. A special experiment, which including the JEBAR term but without wind stress, gave a more than 40 Sv transport at the same location. Therefore the maximal transport in the regime of the Gulf Stream recirculation obtained from low-resolution model is primarily from the JEBAR term. Accordingly, the total meridional circulation rate, as defined in this study, in the North Atlantic, including the contribution of the meridional throughflow, horizontal wind-driven gyres, and other deep recirculation gyres, may be on the order of 100 Sv.

[24] The most interesting feature of the North Atlantic Subtropical Gyre is its two-center structure in the upper

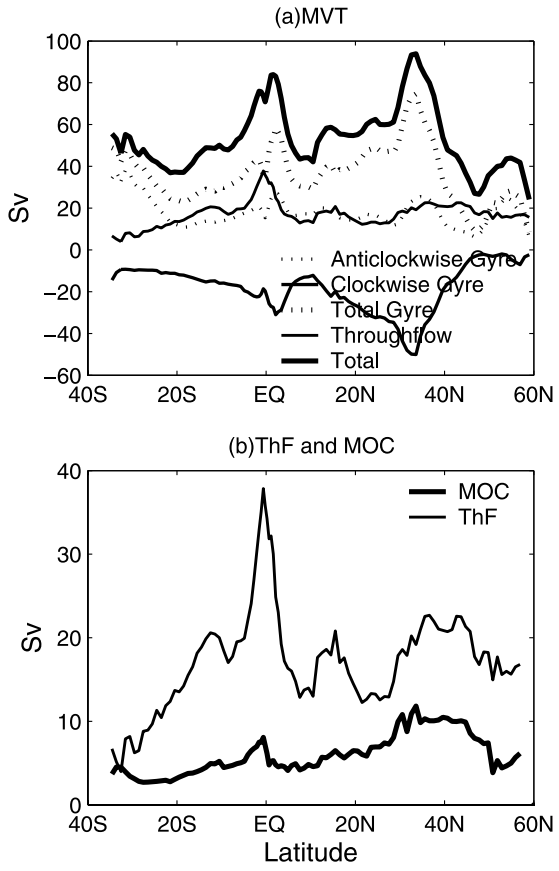

Figure 4. (a) Climatological mean depth-integrated northward volume transports due to different components in the Atlantic, in units of Sv. The solid line below zero on the horizontal axis is the volume transport due to clockwise gyration (plotted as negative in this figure). The dotted line above zero on the horizontal axis for the anticlockwise gyration, and the elongated dotted line is the total contribution due to gyration. The thin solid line above the horizontal axis is for the throughflow, and the thick solid line is the total meridional circulation. (b) Climatological mean throughflow (thin solid line) and MOC (thick solid line).

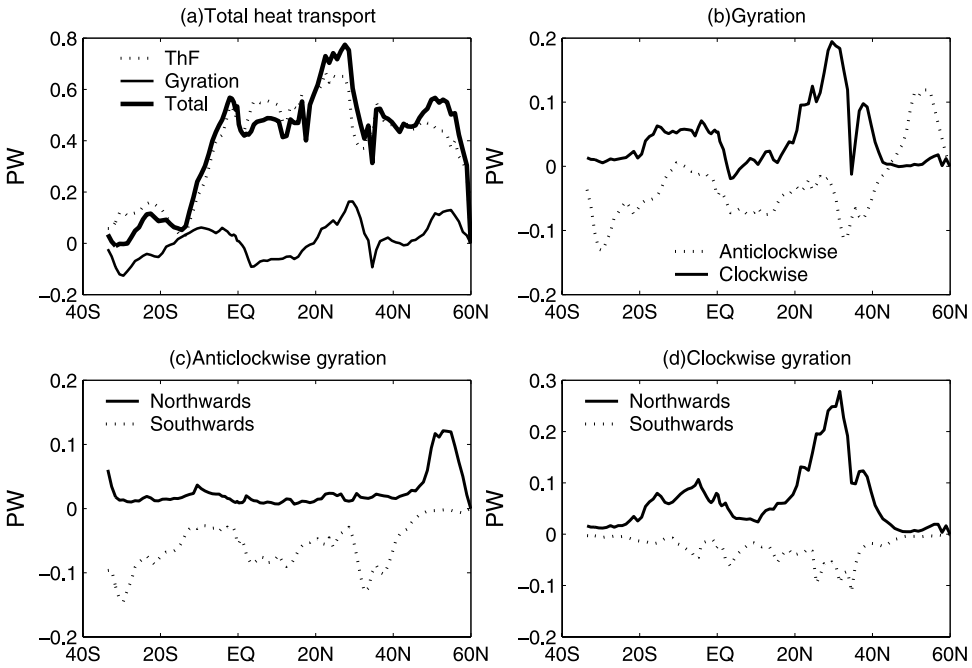

Figure 5. Climatological mean depth-integrated northward heat transports due to different components, in units of PW (10^{15} W). (a) The total heat flux; the dotted line is the meridional throughflow, the thin solid line is the gyration, and the thick solid line is the total heat transport. (b) The northward heat transport due to gyration. (c) The northward/southward heat transport due to anticlockwise gyration. (d) The northward/southward heat transport due to clockwise gyration.

ocean (Figure 3a). The major center is located at latitudes of the Gulf extension (30–40°N), where thermocline is the deepest. This feature is the well-known northern intensification of the wind-driven circulation, which is associated with the strong recirculation there. The maximum transport due to gyration here can reach 75 Sv (Figure 4a). The strong circulation in this region is associated with the large bottom pressure torque generated by the strong interaction of flow and topography near the Mid-Atlantic Ridge [*Sarkisyan and Ivanov*, 1971; *Holland*, 1973; *Greatbatch et al.*, 1991].

[25] The second center is located at latitudes of 20–30°N close to the latitude of the Florida Strait. Although the main thermocline here is relatively shallow, the transport is a local maximum, which is mainly due to strong wind stress curl, and this can be clearly identified from maps of dynamic height anomaly or the Sverdrup transport (Figure 2). The meridional volume transport due to gyration associated with this center (integrated over the top 1500 m) is about 25 Sv, which compares favorably with the Sverdrup relation and with the observed transport [*Niiler and Richardson*, 1973]. Because of the low resolution of the numerical model, however, this second center of gyration appears as a weak local maximum (Figure 4a).

[26] The center of meridional volume transport of the Angola Gyre is located at 4°S and depth of 100 m (Figure 3a), with a depth-integrated volume flux of 7.5 Sv. In comparison, previous studies suggested that the thermal center of Angola Dome is at 13°N, and the associated depth-integrated volume flux is 5 Sv [*Gordon and Bosley*, 1991; *Yamagata and Iizuka*, 1995]. Note that data used in our study is taken from a numerical model that includes the effect of realistic topography, friction, and more accurate equatorial circulation. In the volume transport pictures the northern edge of Angola Gyre consists of subsurface equatorial currents, which may not be captured accurately in the depth-integrated volume flux calculation based on wind stress by *Gordon and Bosley* [1991].

[27] The clockwise Guinea Gyre is centered at (8°N, 100 m) with north–south extant 8° and the base of this gyre is 200 m below the sea surface (Figure 3b), with the depth-integrated meridional transport of 5 Sv. The center of the anticlockwise Subpolar Gyre is near 54°N and 640 m below the sea surface (Figure 3b). The meridional volume flux integrated over the upper 1500 m is approximately 20 Sv. Note that the vertical gradient of meridional volume flux of this gyre is relatively small in the upper 1000 m, reflecting the relatively weak stratification at high latitudes. In addition, there is a local maximum of the meridional volume transport due to anticlockwise gyration between 30 and 40°N (Figure 3b), which is not directly linked to the subpolar gyre. In fact, this local maximum is mainly due to the mesoscale eddies in the Iberian Margin region outside of the Mediterranean.

[28] The South Subtropical Gyre is located within 20–35°S (Figures 3b and 4a), with the meridional volume transport of 38 Sv, which is much greater than 20 Sv predicted by the Sverdrup relation. The enhancement of the circulation may be due to the bottom pressure torque, as discussed above for the case of the North Atlantic Subtropical Gyre. In addition, there the circulation intensification may be linked to the interbasin flow associated with the global thermohaline circulation. Input of Agulhas eddies from Indian Ocean contributes about 5 Sv to the south subtropical gyre [*Witter and Gordon*, 1999].

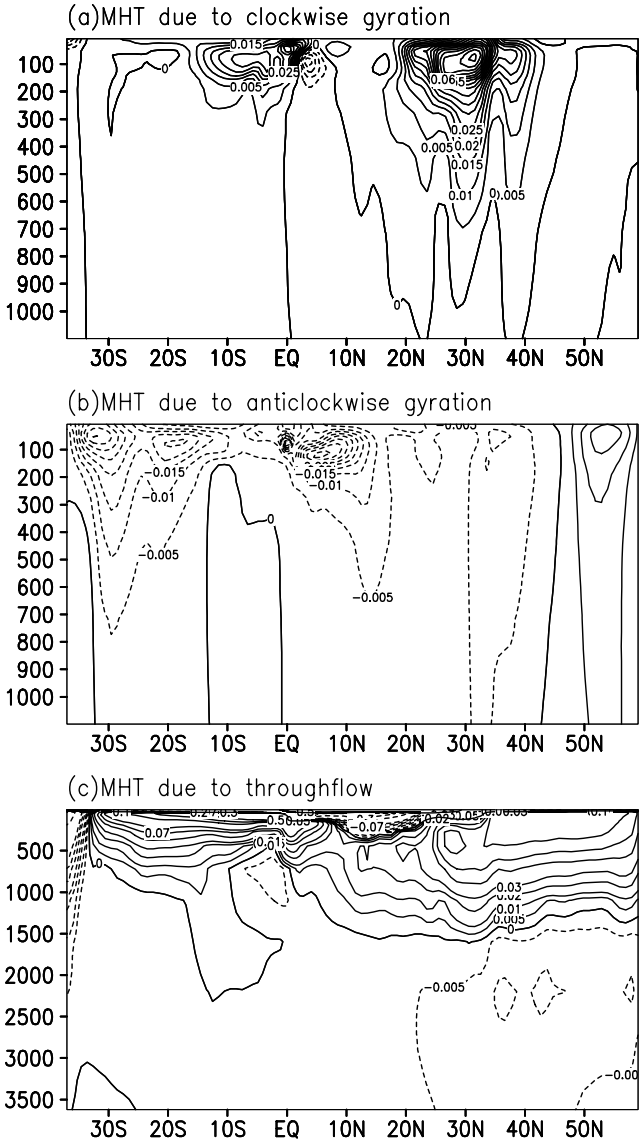

Figure 6. Meridional heat transport (MHT) as a function of latitude and depth due to (a) clockwise gyration, (b) anticlockwise gyration, and (c) throughflow for the Atlantic diagnosed from SODA, in units of PW/100 m.

[29] The meridional distribution of both the newly defined meridional throughflow rate and the commonly used MOC rate is shown in Figure 4b. It is readily seen that the meridional throughflow rate is much larger than the MOC rate.

3.3. Meridional Heat Flux

[30] The total amount of poleward heat flux in the Atlantic basin is estimated as 0.8 PW [*Trenberth and Caron*, 2001]. In this study the total poleward heat flux in the ocean is separated into two major components. For the climatological state diagnosed from SODA data the flux associated with the meridional throughflow reaches a maximum of 0.65 PW around 28°N and the horizontal gyration 0.2 PW around 30°N (Figures 5 and 6). Note that throughflow includes contribution due to multiple cells in the vertical direction thus it is a better description of the circulation physics, compared with the commonly used MOC rate.

[31] Although the meridional throughflow is the major contributor, the contribution of gyration is not negligible. Meridional heat flux due to throughflow is northward near the equator, owing to the warm cross-equator surface flow. However, both tropical gyres contribute to an equatorward heat flux, but the Subtropical gyres and Subpolar Gyre contribute to a poleward heat flux (Table 1). The poleward heat flux in the North Atlantic reaches its maximum around 28°N, where contribution due to both throughflow and gyration are larger (Figure 5a). The component associated with throughflow is slightly weaker because of the data quality of SODA package. In particular, total poleward heat flux in the South Atlantic is smaller than the values reported in previous studies [*Trenberth and Caron*, 2001].

[32] The northward heat flux due to the gyration can be separated into two components associated with clockwise and anticlockwise gyres (Figure 5b). The poleward heat flux due to the anticlockwise (clockwise) gyre can be further separated into two subcomponents: the northward and southward heat fluxes (Figure 5c and 5d).

[33] The meridional heat transport is mainly confined in the upper 300 m (Figure 6). The center of heat flux of the North Subtropical Gyre is located near 30°N and 100 m below sea level, in contrast to the center of volume flux. Although the volume flux is strong near 27°N, the east-west temperature difference of the basin is quite larger around 33°N because of warm Gulf Stream water and southward cold water near eastern boundary of the basin. The mean depth-integrated heat flux of this gyre is about 0.2 PW, which is about 1/3 of that of throughflow at the same latitude. Heat flux map for the South Subtropical Gyre apparently has two maxima, as shown clearly in Figure 6b, in contrast to the single center structure in the map of volume flux (Figure 3b).

[34] The Guinea Gyre is more active in absorbing heat across the air-sea interface in the tropics because it is cooled by the wind-driven upwelling. This gyre is associated with an equatorward heat flux about 0.06 PW, integrated over the upper 200 m (Table 1). The maximum heat flux is centered near 5–10°N and 120 m below sea surface (Figure 6b). It seems clear that heat flux per unit volume transport associated with the Guinea Gyre is much larger than that of the Subtropical and Subpolar gyres, which can be linked to the strong zonal temperature gradient associated with the cold tongue in the Guinea Gyre. Although the Angola Gyre is also located in tropical region, with a slightly larger volume flux, the heat flux it carried is the same as that of the Guinea Gyre.

4. Interannual-Decadal Variability

4.1. Sverdrup Function With Time Delay

[35] For a steady circulation, the meridional volume transport of the wind-driven gyres obeys

$$M = -\frac{f}{\beta}\int_{\lambda}^{\lambda_e} w_e r\cos\phi d\lambda \tag{20}$$

$$w_e = \frac{1}{r\rho_0 f}\left(\frac{1}{\cos\phi}\frac{\partial\tau^{\phi}}{\partial\lambda} - \frac{\partial\tau^{\lambda}}{\partial\phi} + \frac{\tau^{\lambda}}{\sin\phi\cos\phi}\right), \tag{21}$$

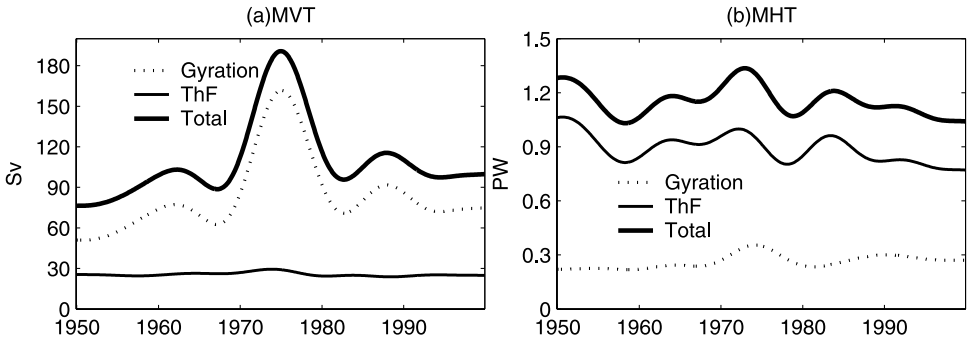

Figure 7. Decadal variability of the maximal poleward fluxes in the Atlantic, within the latitudinal band of 20–40°N for (a) volume flux (Sv) and (b) heat flux (PW). The thin solid line is from throughflow, the dotted line is from the gyration (the sum of clockwise and anticlockwise gyres), and the thick solid line is from total poleward fluxes.

where w_e is the Ekman pumping rate, $f = 2\Omega\sin\phi$ is the Coriolis parameter, $\beta = df/rd\phi$, r is the radius of the Earth, Ω is the Earth's angular velocity, ϕ is the latitude, λ is the longitude, and τ^{ϕ} and τ^{λ} are the meridional and longitudinal components of wind stress, respectively.

[36] Equation (20) applies to steady circulation only. When wind stress changes with time, the circulation adjusts with a time delay. The circulation is completely established after all baroclinic Rossby waves reach the western boundary of the basin; however, the arriving of the first baroclinic Rossby waves initiated from the eastern boundary indicates the nearly completion of the adjustment at each station. Therefore the corresponding formula is

$$M(t) = -\frac{f}{\beta}\int_{\lambda}^{\lambda_e} w_e\left[\lambda, \phi, t - r\cos\phi(\lambda_e - \lambda)/c_g\right] r\cos\phi d\lambda, \tag{22}$$

where $c_g = \beta R_e^2$ is the group velocity of Rossby waves [*Chelton et al.*, 1998; *Yang and Liu*, 2003],and R_e is the first baroclinic radius of deformation. The time correction term represents the time delay due to Rossby wave propagation.

[37] A recent study by *Hirschi et al.* [2007] suggested that in an eddy-permitted model the effect of the time delay in the response to the Rossby wave signal crossing the basin can be quite significant in intraseasonal timescales; however, because of the relatively low resolution used in generating SODA data analyzed in this study, such an important dynamic effect may not be fully realized.

4.2. Decadal Variability of Gyres in the North Atlantic

[38] The maximal meridional circulation rate and the corresponding maximal poleward heat flux associated with gyration and throughflow in the Atlantic (both maximal were defined between 20 and 40°N) vary greatly over decadal timescales (Figure 7). Note that contribution due to mesoscale eddies in the Iberian Margin region in the eastern Atlantic Ocean (more than 10 Sv) is calculated separately (figure not included).

[39] The most outstanding feature is the dramatic intensification of gyration in the 1970s, apparently associated with the regime shift in the atmospheric circulation around 1975–1976. Although the volume flux associated with throughflow remains virtually constant, the maximal meridional volume flux associated with gyration (the sum of clockwise and anticlockwise gyres) went up from ~60 to ~160 Sv, more than doubled during this time period. In addition, there seems a gradual intensification of gyration over the past 50 years. Our results diagnosed from the SODA data indicate the intensification of the gyration associated with the regime shift, which is opposite to the weakening of Gulf Stream recirculation discussed in some previous publications [e.g., *Ezer et al.*, 1995].

[40] Poleward heat flux associated with throughflow and gyration changed greatly over the past 50 years. There is a clear trend of decline in poleward heat flux associated with throughflow. In particular, there is a large amplitude change that took place in the 1970s and 1980s; the contributions due to both gyration and meridional throughflow went up from 1.1 to 1.35 PW (Figure 7b), although the corresponding volume transport increase in the meridional throughflow was relatively small (Figure 7a). Note that heat flux plotted in Figure 7 is based on maximal flux found over 12 months of each years and between 20 and 40°N; thus values in Figure 7 are noticeably larger than those plotted in Figure 5.

[41] This change in heat flux is due to large changes in the thermal structure in the upper ocean associated with the wind-driven circulation in response to the regime shift in the 1970s. A previous study by *Häkkinen* [1999] indicated an increase of poleward heat flux on the order of 0.2 PW during the regime shift in 1970s, so our result is consistent with her simulation. However, her simulation suggested that the poleward heat flux has a clearly defined upward trend over the past 50 years, while our result indicated a general weakening trend, especially for the last two decades. The reason for such description remains unclear, and should be explored in further study.

[42] The regime shift seems to have a noticeable impact on the poleward heat flux associated with gyration in the 1970s. The maximal poleward heat transport due to gyration went up from 0.2 to 0.36 PW. In addition, there is a linear trend of increased poleward heat flux associated with gyration over the past 50 years. Although, the overall trend of poleward heat flux is a slight decline over the past 50 years due to the weakening of contribution associated with the throughflow.

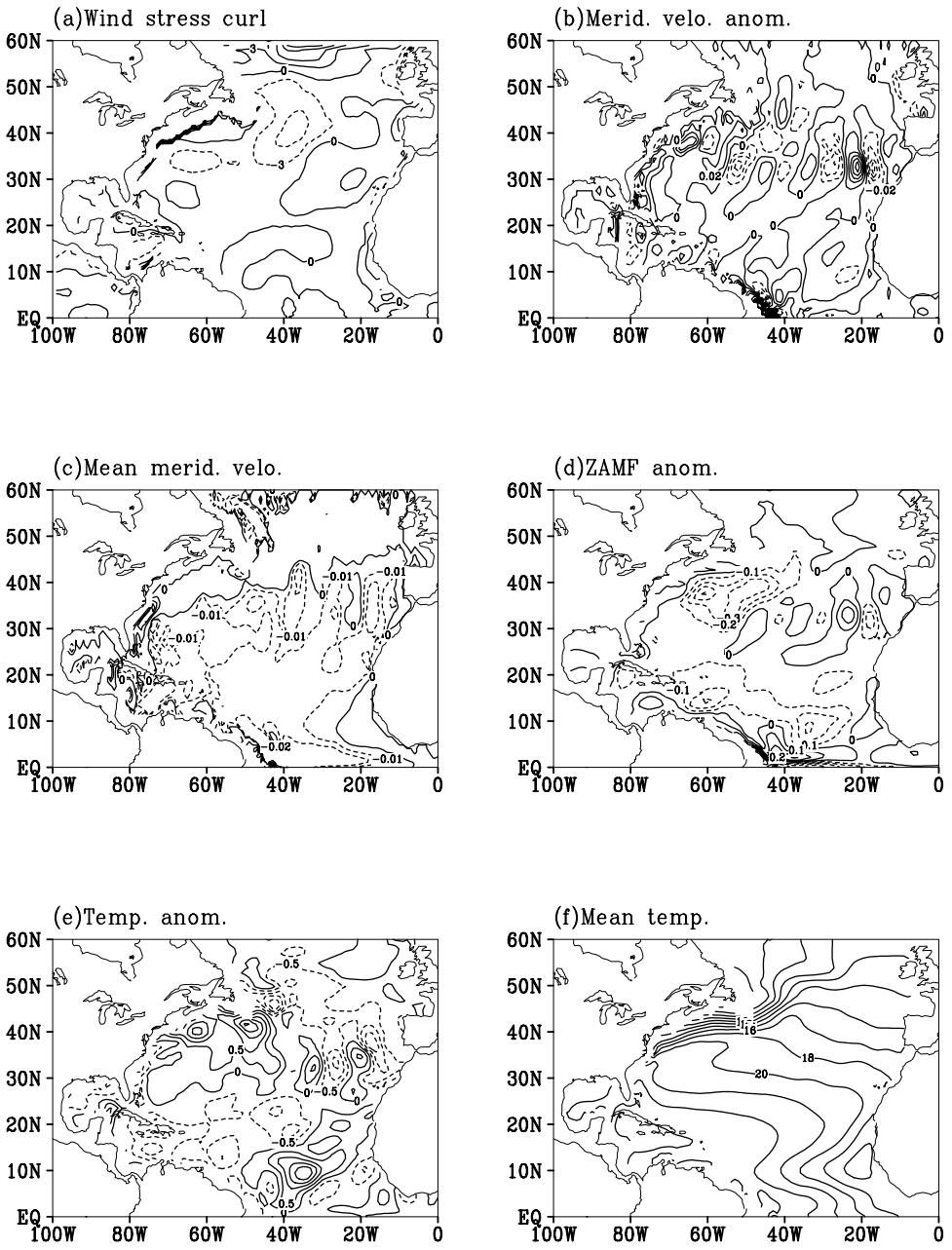

Figure 8. Flow field anomaly (year 1976 minus climatology) and the corresponding climatological mean, all for level 82.5 m except Figure 8a, for (a) wind stress curl anomaly ($\times 10^{-8}$ N m^{-3}, contour intervals are 3 N m^{-3}), (b) meridional velocity anomaly (ms^{-1}, contour intervals are 0.02 ms^{-1}), (c) climatological mean meridional velocity (ms^{-1}, contour levels are -0.02, -0.01, 0, 0.1, 0.2, 0.3, 0.4, and 0.5), (d) ZAMF anomaly (Sv, contour intervals are 0.1 Sv), (e) temperature anomaly (°C, contour intervals are 0.5°C), and (f) climatological mean temperature (°C).

[43] The regime shift happened near 1976 was a basin-scale reorganization of the forcing and circulation in the Atlantic Ocean, and many aspects of such changes can be identified from the SODA data as well. Our discussion here will be focused on the North Atlantic Ocean south of 60°N (Figure 8). For example, in year 1976, wind stress curl anomaly appeared as positive in the eastern part of the North Atlantic Ocean and negative in the western part of the basin (Figure 8a). Wind stress curl anomaly gave rise to meridional velocity anomaly (Figure 8b) and zonal-accumulated meridional volume flux anomaly (Figure 8d). It is readily seen that the anticyclonic gyre in the subtropical basin was intensified, especially in the northwest corner; however, there were also large eddy-like anomalous features in the eastern basin. According to the working definition adapted in this study, these anomalous features can all contribute to the gyration part of the meridional transport; however, their contribution to the poleward heat flux can have opposite signs, which can be explained as follows.

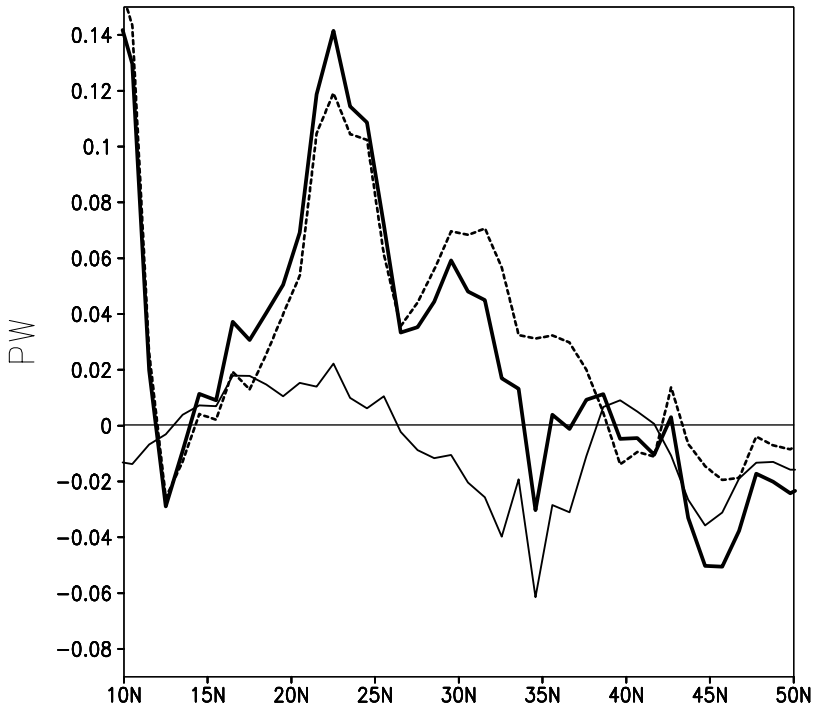

Figure 9. Zonally integrated poleward heat flux anomalies (PW) (year 1976 minus climatology) for the 82.5 m level. The thin solid line is the temperature anomaly advected by mean velocity, the dotted line is the mean temperature advected by velocity anomaly, and the thick solid line is the total poleward heat flux anomaly.

[44] First, changes in velocity structure are closely associated with changes in the temperature distribution. For example, corresponding climatological mean temperature and its anomaly are included in Figures 8f and 8e, respectively. By definition, poleward heat flux is proportional to the product of meridional velocity and temperature; thus, anomaly of poleward heat flux at a give level consists of two components

$$c_p \rho_o \left(\int_{x_w}^{x_e} T' \overline{v} dx \Delta z + \int_{x_w}^{x_e} \overline{T} v' dx \Delta z \right), \tag{23}$$

i.e., the anomalous temperature advected by the mean meridional velocity and the mean temperature advected by the anomalous meridional velocity. Comparing Figures 8c and 8e, it is readily seen that around 25–40°N in the western basin the first term is dominated by positive temperature anomaly in the interior being advected equatorward, so that the heat flux anomaly is negative. In the eastern basin, this heat flux term may be rather small because of cancellation of positive and negative contributions.

[45] On the other hand, there is an outstanding anticyclonic gyre anomaly (Figure 8d) in the western basin for the latitudinal band of 20–40°N. Combining with a negative zonal gradient of the climatological mean temperature (Figure 8f), this gives rise to a positive poleward heat flux anomaly. In comparison, circulation anomaly in the eastern basin appears in forms of large eddy-like features, so their contribution to poleward heat flux may cancel each other. As a result, there is a large positive heat flux anomaly due to the combination of meridional velocity anomaly (in forms of intensified anticyclonic gyration) and climatological mean temperature at this latitude band.

[46] Contributions from these two terms for the 82.5 m level are plotted in Figure 9. It is clear that the contribution due to the anomalous gyration is the dominating contributor to the poleward heat flux anomaly during the 1970s regime shift. Change of the poleward volume flux and poleward heat flux for the top 1000 m, as diagnosed from SODA, are included in Figure 10. It is readily seen that there are great changes for the latitudinal band of 20–35°N during this time, as compared with climatology.

[47] Given the quality of SODA data in the South Atlantic, only decadal variability of gyration in the North Atlantic (the North Subtropical Gyre, the Subpolar Gyre, and the Guinea Gyre) are discussed below.

4.2.1. North Subtropical Gyre

[48] As discussed above, the North Subtropical Gyre has two centers, and the circulation around 33°N is deeper and stronger than that around 27°N. Variability in the volume fluxes associated with two centers is different (Figures 11a and 11b). At both latitudes, decadal variability in the volume fluxes was very strong during late 1950s to early 1960s, 1970s, and late 1980s. In particular, gyration rate changed greatly in the 1970s, which is apparently a direct response to the regime shift in the atmospheric circulation in 1975–1976. Variability in maximal meridional circulation rate diagnosed from the numerical model is much stronger than that diagnosed from the Sverdrup relation. This large difference is due to the fact that the former includes contribution due to horizontal wind-driven gyres, in partic-

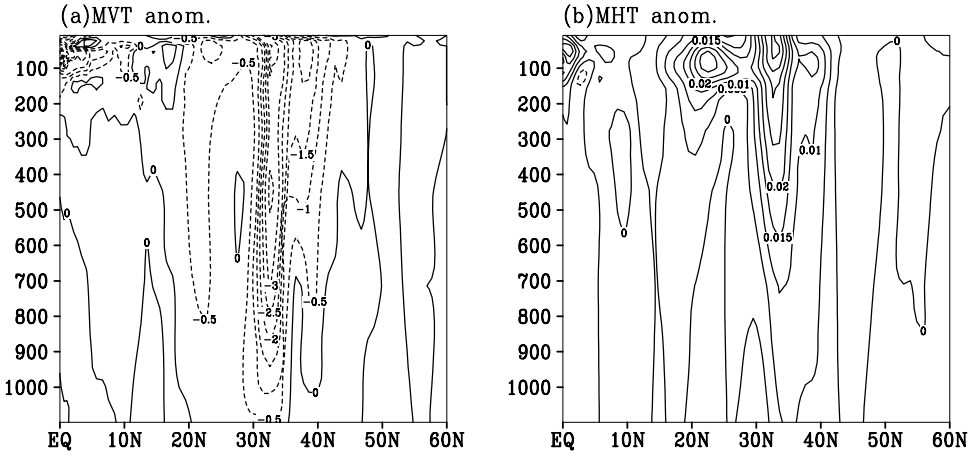

Figure 10. Transport anomaly (year 1976 minus climatology) for (a) meridional volume transport (MVT) anomaly (Sv) and (b) meridional heat transport (MHT) anomaly (PW/100 m) due to clockwise gyres as a function of latitude and depth.

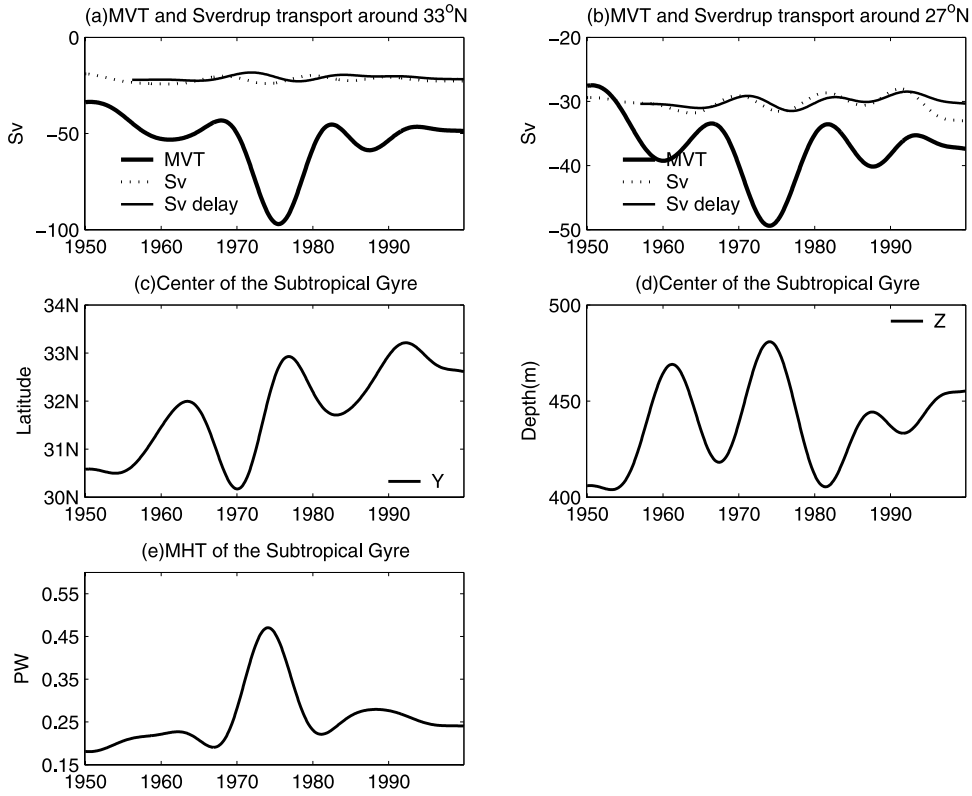

Figure 11. Decadal variability of the North Subtropical Gyre in the Atlantic Ocean. The maximal depth-integrated volume flux (a) between 30 and 40°N and (b) between 20 and 28°. The thick solid line for the 8-year low passed filtered depth-integrated meridional transport (plotted as negative because the component associated with the Sverdrup flow is southward), the light solid line for the 8-year low passed filtered Sverdrup transport with time delay, and the dotted line for the Sverdrup transport without time delay. (c) The 8-year low passed filtered latitudinal center (labeled as Y) of the volume transport corresponding to latitudes of maximal depth-integrated meridional volume transport between 30 and 40°N. (d) The 8-year low passed filtered depth of the center (labeled as Z) of the volume transport. (e) The 8-year low passed filtered maximal northward heat transport (PW) associated with the North Subtropical Gyre between 20 and 40°N.

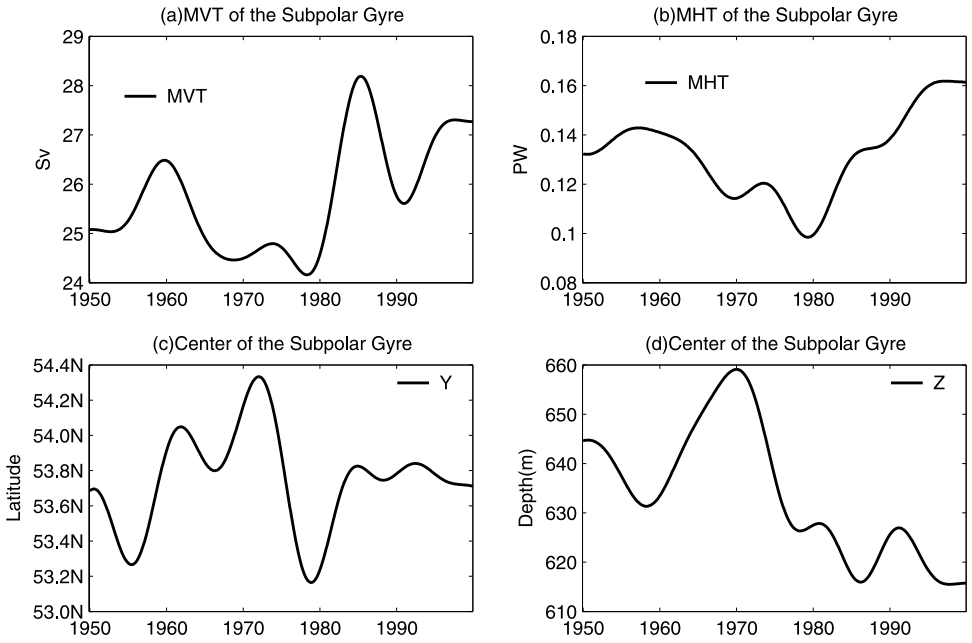

Figure 12. Decadal variability of the Subpolar Gyre in the Atlantic Ocean. (a) The 8-year low passed filtered maximal depth-integrated meridional volume transport (Sv) between 50 and 60°N. (b) The 8-year low passed filtered maximal northward heat transport (PW) between 50 and 60°N. (c) The 8-year low passed filtered latitudinal center of the volume transport corresponding to latitudes of maximal depth-integrated meridional volume transport between 50 and 60°N. (d) The 8-year low passed filtered depth of the center of the volume transport.

ular, the contribution due to the bottom topographic torque in the Gulf Stream recirculation regime.

[49] Assuming the zonal temperature gradient remains constant, strong gyration is generally associated with strong poleward heat flux. In addition, strong gyration is associated with northward and downward migration of the center, compared with the normal position. There is apparently a large shift of both the meridional position and depth of the gyre center in the 1970s, just before and after the regime shift in atmospheric circulation (Figures 11c and 11d).

[50] The poleward heat flux also went through a major change in the 1970s. Although the climatological mean value of the heat flux is about 0.25 PW, it reached a value of more than 0.45 PW in the middle of 1970s. Overall, there was a clearly defined trend in the Subtropical Gyre over the past 50 years: the gyre intensified, its center moved northward and to a deeper level; at the same time it transported more heat poleward. In particular, the regime shift in the atmospheric circulation in 1975–1976 has had a major impact on the Subtropical Gyre.

[51] In the early 1950s, the depth-integrated volume flux around 27°N (Figure 11b) was close to the prediction by the Sverdrup relation with or without time delay; however, there is a large difference between these fluxes starting from 1960s. This difference indicates that although wind-driven gyre at this latitude is primarily controlled by the wind stress curl, there are other mechanisms that also regulate the strength of gyration here. While around 33°N the depth-integrated volume flux is much stronger than that calculated from the Sverdrup relation. Other mechanisms, such as bottom pressure torque on the western side of the Mid-Atlantic Ridge, can enhance the transport of the Subtropical Gyre.

4.2.2. Subpolar Gyre

[52] The depth-integrated meridional volume flux, heat flux, and the center of the Subpolar Gyre varied greatly over the past 50 years (Figure 12). The center of the gyre is located at about 53.8–54°N, with strongest transport in 1960, 1984–1985, and 1994–1995. The center of Sverdrup circulation of Subpolar Gyre is at about 60°N (not shown). For the Subpolar Gyre the effect of bottom pressure torque forcing is to displace the Subpolar Gyre southward rather than enhance its transport [*Greatbatch et al.*, 1991]. Because of the limitation of SODA data the structure of the circulation related to this gyre is incomplete.

[53] There are also three peaks of the heat transport of the Subpolar Gyre: the 1960s, 1980s, and 1990s. There was a clear trend of rapid incline during the early 1980s, consistent with the results from the volume flux of this gyre. Note that heat flux increased 60% over this period, which was much larger in comparison with an increase in volume flux of 10%. This implies a large increase in the zonal temperature difference during the same period.

[54] With the volume and heat fluxes increasing the depth center of this gyre moved upward after 1970. This means that the upper stratification becomes stronger and thermocline becomes shallower. The meridional migration of this gyre was much smaller than that of the Subtropical Gyre.

4.2.3. Guinea Gyre

[55] Decadal variations of volume and heat fluxes of the Guinea Gyre show similar trends (Figure 13): the circulation was strong in 1960–1990 and weak in 1950s and 1990s. On decadal timescales the trend of the diagnosed volume flux is

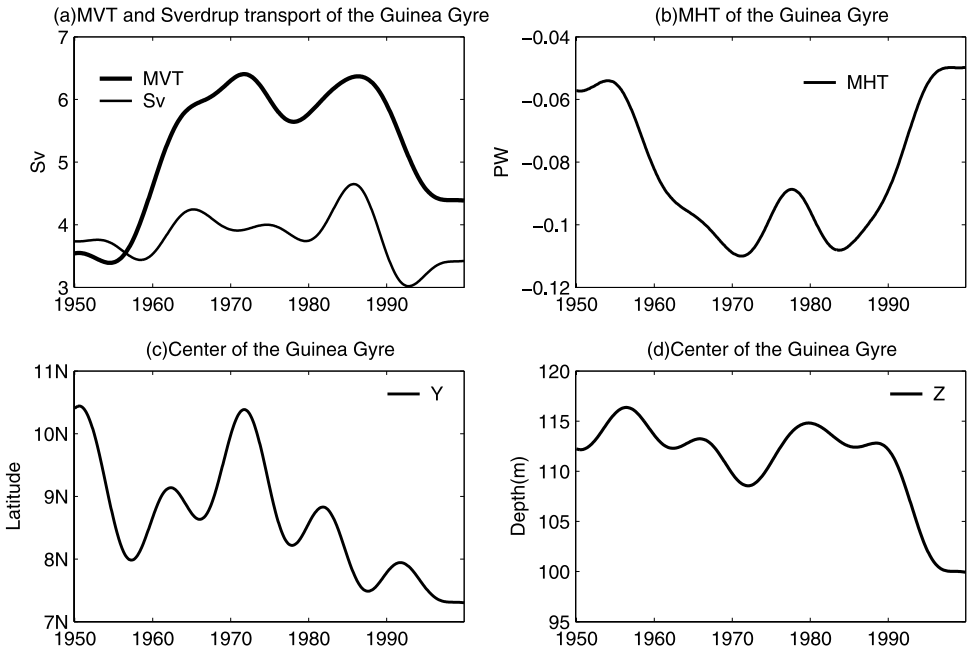

Figure 13. Decadal variability of the Guinea Gyre in the Atlantic Ocean. (a) The thick solid line for the 8-year low passed filtered maximal depth-integrated meridional volume transport between 5 and 13°N. The light solid line for the 8-year low passed filtered maximal Sverdrup transport between 5 and 13°N, without time delay. (b) The 8-year low passed filtered maximal depth-integrated meridional heat transport between 5 and 13°N. (c) The 8-year low passed filtered latitudinal center of the volume transport, corresponding to latitudes of maximal depth-integrated meridional volume transport between 5 and 13°N. (d) The 8-year low passed filtered depth of the center of the volume transport.

different from that of the Sverdrup transport. In particular, the diagnosed volume flux increased greatly over the period of 1960–1990; however, volume flux calculated from the modified Sverdrup relation increased only slightly over the same period. Note that the regime shift around 1975–1976 does not seem to have much impact on the gyration rate of the Guinea Gyre, and it is quite different from what happened in the North Subtropical Gyre.

[56] The Guinea Gyre is located within the upwelling region near the coast of the eastern tropical Atlantic. Besides local wind stress curl, remote forcing due to poleward coastal Kelvin wave is an important contributor to the wind-driven gyres [*Siedler et al.*, 1992; *Yamagata and Iizuka*, 1995] at seasonal timescales, especially for the meridional volume transport. For example, in the early 1950s the diagnosed volume flux of the Guinea Gyre was the same as that from the Sverdrup function. However, after the late 1950s the diagnosed volume flux became much larger than that from the Sverdrup relation. Therefore such changes are not directly linked to wind stress changes; instead, they may be linked to Kelvin wave activity, as discussed above.

[57] The Angola Gyre also has a peak during the same period (figure not included). The volume transport variation of the Guinea Gyre was weaker than that of the Angola Gyre, and this may be due to the fact that much of the energy carried by the poleward Kelvin waves in the Guinea basin is lost within the gulf, but the corresponding loss of energy in the Angola basin is much smaller due to the relatively smooth coastline.

[58] As the volume flux intensified over the period of 1960–1990, the equatorward heat flux associated with the gyration also intensified (Figure 13b). Over the past 50 years the center of the Guinea Gyre gradually migrated equatorward and upward (Figures 13c and 13d).

5. Summary and Discussion

[59] Poleward transport of mass, heat, and freshwater through the oceanic circulation is one of the vital components in the climate system. Changes in climate are closely related to variations of these poleward fluxes. Although poleward heat flux and its contribution to climate have been studied in many previous publications, many aspects of these fluxes remain poorly understood.

[60] In this study we explored the contribution of wind-driven gyration to poleward volume and heat transports. Using a new diagnostic tool, we have been able to separate the poleward transports of volume and heat into two components: the throughflow and the gyration. In a broad sense the throughflow is induced by the thermohaline circulation, and the gyration is induced by the wind-driven circulation; however, in the ocean the thermohaline and wind-driven circulation are closely linked to each other and thus cannot be separated. Our diagnostic tool can provide more accurate information about the contribution to the poleward volume and heat fluxes due to wind-driven gyres in the oceans. In contrast, the zonally integrated stream function used in many studies cannot convey the important contribution of the wind-driven circulation to the poleward volume flux. Since the poleward heat transport associated

with the wind-driven horizontal gyre is directly proportional to the zonal temperature difference in the basin, changes in the poleward heat flux indicate variation in both the volume transport of the gyre and the horizontal distribution of the temperature in the upper ocean.

[61] The Atlantic Ocean provides a good example for demonstrating the usefulness of this tool. The most interesting results from this study are as follows. First, wind-driven gyres in the Atlantic contribute a noticeable portion to the poleward transports of volume and heat, as discussed in many previous publications [e.g., *Boning and Herrmann*, 1994; *Czaja and Marshall*, 2006]; second, the regime shift in the atmospheric circulation in the 1970s induced great changes in both the strength of the North Atlantic Subtropical Gyre and the poleward heat associated with this gyre. Our diagnosis indicated that both the volume flux and the poleward heat flux associated with the Subtropical Gyre doubled during the middle of 1970s.

[62] The diagnostics in this study is based on the output of numerical model, so the details of the results are sensitive to the parameterization of the model and some specific choice made in the model. However, the basic concepts and diagnostic tool discussed here are applicable to other data sets.

[63] Poleward heat transport has been discussed in many previous studies, and our study is focused on the partition of the heat flux among the throughflow and the wind-driven gyration. Because of the low resolution used in generated the data set, contribution due to transient eddies was excluded from our discussion; although, it is well known that eddies can make a noticeable contribute to poleward heat flux. Although the discussion here is focused on the projection onto the *y-z* plane, this technique may also apply to the *x-z* plane or other coordinates, such as the density coordinates or the potential temperature coordinates.

[64] This new technique will be used to diagnose the circulation in the world oceans, such as the circulation in the Pacific Ocean and the Indian Ocean. In this way, we hope to construct a complete picture of the dynamic role of the wind-driven gyres in the world ocean circulation and climate, and, in particular, the climate variability in connection of the wind-driven gyres in the upper 1 km of the world oceans.

[65] **Acknowledgments.** J.H. and H.W. were jointly supported by The National Natural Science Foundation of China (40406004, 40531006) and by the National Hi-Tech Project (“863” program) of China under contract 2006AA09Z158. R.X.H. was supported by the Van Alan Clark Chair of the Woods Hole Oceanographic Institution. Critical comments from reviewers and Editor James Richman helped us to improve the presentation of this study.

References

Boning, C. W., and P. Herrmann (1994), On the annual cycle of poleward heat transport in the ocean: Results from high resolution modeling of the North and Equatorial Atlantic, *J. Phys. Oceanogr.*, *24*, 91–107.

Brady, E. C. (1994a), Interannual heat transport in a numerical model of the Pacific equatorial upwelling zone, *J. Phys. Oceanogr.*, *24*, 2675–2694.

Brady, E. C. (1994b), The seasonal cycle of meridional heat transport in a numerical model of the Pacific equatorial upwelling zone, *J. Phys. Oceanogr.*, *24*, 2658–2673.

Broecker, W. S. (1991), The great ocean conveyor, *Oceanography*, *4*, 79–89.

Bryan, K. (1982), Poleward heat transport by the ocean, *Ann. Rev. Earth Planet. Sci.*, *10*, 15–38.

Bryden, H. L., and M. M. Hall (1980), Heat transport by currents across 25°N latitude in the Atlantic Ocean, *Science*, *207*, 884–886.

Busalacchi, A. J., and J. Picaut (1983), Seasonal variability from a model of the tropical Atlantic Ocean, *J. Phys. Oceanogr.*, *13*, 1564–1588.

Carton, J. A., G. Chepurin, and X. Cao (2000a), A Simple Ocean Data Assimilation analysis of the global upper ocean 1950–1995: part II: Results, *J. Phys. Oceanogr.*, *30*, 311–326.

Carton, J. A., G. Chepurin, X. Cao, and B. S. Giese (2000b), A Simple Ocean Data Assimilation analysis of the global upper ocean 1950–1995: part I: Methodology, *J. Phys. Oceanogr.*, *30*, 294–309.

Chelton, D. B., R. A. deSzoeke, M. G. Schlax, K. E. Naggar, and N. Siwertz (1998), Geographical variability of the first-baroclinic Rossby radius of deformation, *J. Phys. Oceanogr.*, *28*, 433–460.

Czaja, A., and J. Marshall (2006), The partitioning of poleward heat transport between the atmosphere and ocean, *J. Atmos. Sci.*, *63*, 1498–1511.

Dickson, R. R., and J. Brown (1994), The production of North Atlantic Deep Water: Sources, rates, and pathways, *J. Geophys. Res.*, *99*(C6), 12,319–12,341.

Ezer, T. (1999), Decadal variabilities of the upper layers of the subtropical North Atlantic: An ocean model study, *J. Phys. Oceanogr.*, *29*, 3111–3124.

Ezer, T., G. L. Mellor, and R. J. Greatbatch (1995), On the interpentadal variability of the North Atlantic Ocean: Model simulated changes in transport, meridional heat flux and coastal sea level between 1955–1959 and 1970–1974, *J. Geophys. Res.*, *100*(C6), 10,559–10,566.

Fanning, A. F., and A. J. Weaver (1997), A horizontal resolution and parameter sensitivity study of heat transport in an idealized coupled climate model, *J. Clim.*, *10*, 2469–2478.

Gordon, A. L., and K. T. Bosley (1991), Cyclonic gyre in the tropical South Atlantic, *Deep Sea Res.*, *38*, 323–343.

Greatbatch, R. J., A. F. Fanning, A. D. Goulding, and S. Levitus (1991), A diagnosis of interpentadal circulation changes in the North Atlantic, *J. Geophys. Res.*, *96*(C12), 22,009–22,023.

Häkkinen, S. (1999), Variability of the simulated meridional heat transport in the North Atlantic for the period 1951–1993, *J. Geophys. Res.*, *104*(C5), 10,991–11,007.

Hirschi, J. J.-M., P. D. Killworth, and J. R. Blundell (2007), Subannual, seasonal, and interannual variability of the North Atlantic meridional overturning circulation, *J. Phys. Oceangr.*, *37*, 1246–1265.

Hogg, N. G., and W. E. Johns (1995), Western boundary currents: U.S. National Report to International Union of Geodesy and Geophysics 1991–1994, *Rev. Geophy.*, *33*, suppl., 1311–1334.

Holland, W. R. (1973), Baroclinic and topographic influences on the transport in western boundary currents, *Geophys. Fluid Dyn.*, *4*, 187–210.

Kushnir, Y. (1994), Interdecadal variations in North Atlantic sea surface temperature and associated atmospheric conditions, *J. Clim.*, *7*, 142–157.

Levitus, S. (1989a), Interpentadal variability of salinity in the upper 150 m of the North Atlantic Ocean, 1970–1974 versus 1955–1959, *J. Geophys. Res.*, *94*(C7), 9679–9685.

Levitus, S. (1989b), Interpentadal variability of temperature and salinity at intermediate depths of the North Atlantic Ocean, 1970–1974 versus 1955–1959, *J. Geophys. Res.*, *94*(C5), 6091–6131.

Mazeika, P. A. (1967), Thermal domes in the eastern tropical Atlantic Ocean, *Limnol. Oceanogr.*, *12*, 537–539.

McCartney, M. S., and L. D. Talley (1984), Warm-to-cold water conversion in the northern North Atlantic Ocean, *J. Physical Oceanogr.*, *14*, 922–935.

Molinari, R. L., D. A. Mayer, J. F. Festa, and H. F. Bezdek (1997), Multiyear variability in the near-surface temperature structure of the midlatitude western North Atlantic Ocean, *J. Geophys. Res.*, *102*(C2), 3267–3278.

Moroshkin, K. V., V. A. Bubnov, and R. P. Bulatov (1970), Water circulation in the eastern South Atlantic Ocean, *Oceanology Engl. Transl.*, *10*, 27–34.

Niiler, P. P., and W. S. Richardson (1973), Seasonal variability of the Florida current, *J. Mar. Res.*, *31*, 144–167.

Sarkisyan, A. S., and V. F. Ivanov (1971), Joint effect of baroclinicity and bottom relief as an important factor in the dynamics of sea currents (in Russian), *Izv. Acad. Sci. USSR Atmos. Oceanic Phys. Engl. Transl.*, *7*(2), 116–124.

Sarmiento, J. L. (1986), On the North and tropical Atlantic heat balance, *J. Geophys. Res.*, *91*(C10), 11,677–11,689.

Schmitz, W. J. (1995), On the interbasin-scale thermohaline circulation, *Rev. Geophys. Space Phys.*, *33*, 151–173.

Schmitz, W. S., and M. S. McCartney (1993), On the North Atlantic circulation, *Rev. Geophys. Space Phys.*, *31*, 29–49.

Semtner, A. J., Jr., and R. M. Chervin (1988), A simulation of the Global Ocean Circulation with resolved eddies, *J. Geophys. Res.*, *93*(C12), 15,502–15,522.

Siedler, G., N. Zangenberg, R. Onken, and A. Morlière (1992), Seasonal Changes in the Tropical Atlantic Circulation: Observation and Simulation of the Guinea Dome, *J. Geophys. Res.*, *97*(C1), 703–715.

Talley, L. D. (2003), Shallow, intermediate, and deep overturning components of the global heat budget, *J. Phys. Oceanogr.*, *23*, 530–560.

Talley, L. D., J. L. Reid, and P. E. Robbins (2003), Data-based meridional overturning streamfunctions for the global ocean, *J. Clim.*, *16*, 3213–3226.

Trenberth, K. E., and J. M. Caron (2001), Estimates of meridional atmosphere and ocean heat transport, *J. Clim.*, *14*, 3433–3443.

Witter, D. L., and A. L. Gordon (1999), Interannual variability of South Atlantic circulation from 4 years of TOPEX/POSEIDON satellite altimeter observations, *J. Geophys. Res.*, *104*(C9), 20,927–20,948.

Yamagata, T., and S. Iizuka (1995), Simulation of the tropical thermal domes in the Atlantic: A seasonal cycle, *J. Phys. Oceanogr.*, *25*, 2129–2138.

Yang, H., and Z. Liu (2003), Basin modes in a tropical-extratropical basin, *J. Phys. Oceanogr.*, *33*, 2751–2763.

R. X. Huang, Department of Physical Oceanography, Woods Hole Oceanographic Institute, 266 Woods Hole Road, Woods Hole, MA 02543, USA.

H. Jiang and H. Wang, Institute of Climate System, Chinese Academy of Meteorological Sciences, Beijing 100081, China. (hjiang@cams.cma.gov.cn)